

# Marginal and Total Exceedance Probabilities for Environmental Contours

Ed Mackay<sup>a</sup>, Andreas F. Haselsteiner<sup>b,c</sup>

<sup>a</sup>*College of Engineering, Mathematics and Physical Sciences, University of Exeter, Penryn, UK*

<sup>b</sup>*University of Bremen, Institute for Integrated Product Development (BIK), Bremen, Germany*

<sup>c</sup>*ForWind – Center for Wind Energy Research of the Universities of Oldenburg, Hannover and Bremen*

## Abstract

Various methods have been proposed for defining an environmental contour, based on different concepts of exceedance probability. In the inverse first-order reliability method (IFORM) and the direct sampling (DS) method, contours are defined in terms of exceedances within a region bounded by a hyperplane in either standard normal space or the original parameter space. The IFORM and DS contours at exceedance probability  $\alpha$  pass through points with marginal exceedance probability  $\alpha$ . In contrast, the more recent inverse second-order reliability method (ISORM) and highest density (HD) contours are defined in terms of an isodensity contour of the joint density function in either standard normal or original parameter space, where an exceedance is defined to be anywhere outside the contour. Contours defined in terms of the total probability outside the contour are significantly more conservative than contours defined in terms of marginal exceedance probabilities. In this work we study the relationship between the marginal exceedance probability of the highest point along an environmental contour and the total probability outside the contour. It is shown that the marginal exceedance probability of the contour maximum can be orders of magnitude lower than the total exceedance probability of the contour, with the differences increasing with the number of variables. For example, a 50-year ISORM contour for two variables at 3-hour time steps, passes through points with marginal return periods of 635 years, and the marginal return periods increase to 10,950 years for contours of four variables. It is shown that the ratios of marginal to total exceedance probabilities for DS contours are similar to those for IFORM contours. However, the exceedance probabilities of the maximum values along an HD contour are not in fixed relation to the contour exceedance probability, but depend on the shape of the joint density function. Examples are presented to illustrate the impact of the choice of contour on simple structural reliability problems, for cases where the use of contours defined in terms of either marginal or total exceedance probabilities may be appropriate. The examples show that, to choose an appropriate contour method, some understanding about the shape of a structure's failure surface is required.

**Keywords:** Environmental contour, Return value, Extremes, Joint distribution, IFORM, ISORM, Highest density contour, Direct sampling contour

## 1. Introduction

Extreme responses of marine structures are often calculated using the environmental contour method [1, 2]. The environmental contour method provides a computationally efficient approximation to a full long-term analysis [3], sometimes referred to as the ‘all sea states approach’. The method involves first estimating a model for the joint distribution of two or more environmental variables. The joint distribution is then used to calculate a set of points which have equal joint exceedance probability, that define a contour in two dimensions, a surface in three dimensions or a hypersurface in higher dimensions. The set of points is commonly referred to as a contour, regardless of the number of dimensions. The responses of the structure are then estimated at a discrete number of points along the contour, so-called design conditions, and the maximum response along the contour is compared with a maximum allowable response.

Unlike the univariate case, there is no unique definition of multivariate exceedance (see e.g. [4, 5]). Consequently, there are multiple ways to define an environmental contour. The commonly used Inverse First-Order Reliability Method (IFORM) [6] and direct sampling (DS) method [7] are both defined in such a way that the contours at exceedance probability  $\alpha$  pass through the points with marginal exceedance probability  $\alpha$ . In contrast, the more recent Inverse Second-Order Reliability Method (ISORM) [8] and highest density (HD) region method [9] are both defined in terms of the total probability outside the contour. If the same exceedance probability is used to define both types of contour, then the ISORM and HD contours will be significantly more conservative than the IFORM or DS contours. Comparisons between IFORM and DS contours have been presented in previous studies (e.g. [10, 11, 12]). However, the relationship between contours defined in terms of marginal exceedance probabilities and those defined in total exceedance probabilities has not previously been studied in detail, although example comparisons were presented in [9, 8]. The purpose of this article is to quantify the marginal exceedance probabilities associated with ISORM and HD contours. Or, to look at the problem the other way, to calculate the probability that an observation falls anywhere

outside an IFORM or DS contour. Furthermore, we present some examples to illustrate the effect that the choice of environmental contour method can have on some simple structural design problems.

The estimation of the joint distribution of environmental variables is the focus of ongoing research. Methods for modelling the joint distribution include hierarchical conditional models [13, 14, 6, 15, 16], copula models [17, 18, 19, 20], kernel density estimates [21, 22] and conditional extreme value models [23, 24, 25, 26]. In the following we assume that a model has been estimated for the joint distribution and contours are to be derived from the joint distribution. There is a wide range of definitions of environmental contours, such as the isodensity contour methods proposed by Haver [13, 27], NORSO [28, p. 12] and DNV GL [29, Section 3.7.2.4], methods based on joint exceedance regions [24], or methods based on univariate analyses [30]. In the present work we focus on four types of contour, namely IFORM, ISORM, DS and HD contours, due to their analogous definitions in terms of either marginal or total exceedance probabilities.

The article is organised as follows. We start by presenting the definitions of the various types of contour in Section 2. The marginal exceedance probabilities associated with the largest values of each variable on ISORM and HD contours are discussed in Sections 3 and 4. The complementary question of the total probability outside IFORM and DS contours is discussed in Section 5 and 6. Section 7 presents two case studies, to illustrate the effect of using different types of contour in some simplified structural design problems. Finally, conclusions are presented in Section 8.

## 2. Environmental contour definitions

The objective of the environmental contour (EC) method is to find a region of the environmental parameter space (referred to here as the ‘design region’) such that a structure that can withstand all environmental conditions within that region has a probability of failure of less than or equal to  $\alpha$ . The boundary of the design region is referred to as the environmental contour (see Figure 1). The various methods for constructing environmental contours make different assumptions about the shape of the failure region (the region of the environmental parameter space in which the structure fails) and consequently what constitutes an exceedance of the environmental contour. The random nature of the structural response conditional on environmental parameters is not modelled explicitly in the EC method, and instead the structure is assumed to fail whenever the environmental conditions are within the failure region. To account for the effect of neglecting the short-term variability of the response, the contour exceedance probability is adjusted by an ‘inflation factor’ (see [6]). In the following, it is assumed that the contour exceedance probability has already been adjusted to account for short-term variability of the response.

Before presenting the definitions of the environmental contour methods, it is useful to introduce some notation. Consider the joint distribution of a vector of  $n$  random variables,  $\mathbf{X} = (X_1, \dots, X_n)$ , with joint distribution  $F(\mathbf{x}) = \Pr(X_1 \leq x_1, \dots, X_n \leq x_n)$  and marginal distributions  $F_j(x_j) = \Pr(X_j \leq x_j)$ ,  $j = 1, \dots, n$ . The corresponding marginal exceedance probabilities are denoted  $Q_j(x) = 1 - F_j(x)$ . In general, we will use  $\alpha$  to denote an exceedance probability and, where necessary, we distinguish between the marginal exceedance probability,  $\alpha_m$ , and the total probability outside the contour,  $\alpha_t$  (see Figure 2). The exceedance probability used to define a contour (or ‘contour exceedance probability’) is denoted  $\alpha_c$ . The definition of  $\alpha_c$  depends on the type of contour. As described below, IFORM and DS contours are defined in terms of marginal exceedance probabilities, whilst ISORM and HD contours are defined in terms of total exceedance probabilities.

The quantile of  $F_j$  at marginal exceedance probability  $\alpha_m$ , is denoted  $x_{j,\alpha_m}$  and is the solution of  $Q_j(x_{j,\alpha_m}) = \alpha_m$ . The lower and upper bounds of  $X_j$  along a contour at exceedance probability  $\alpha_c$  are denoted  $c_{j,\alpha_c}^L$  and  $c_{j,\alpha_c}^U$ . In many of the examples below we are interested in the upper bound only and will drop the superscript  $U$ . Similarly, when we are considering the values of  $x_{j,\alpha_m}$  and  $c_{j,\alpha_c}$  for the same variable we will drop the subscript  $j$ .

### 2.1. Inverse first-order reliability method (IFORM)

The most commonly applied EC method in marine design is the Inverse First-Order Reliability Method (IFORM) [6]. The method is based on the First-Order Reliability Method (FORM), which is a method to approximate a structure’s failure probability [31, pp. 71-125]. In the FORM approach, usually the Rosenblatt transformation [32] is used to transform the joint distribution of  $X_1, X_2, \dots$ , to independent standard normal variables,  $U_1, U_2, \dots$ . The design point is defined as the highest probability point on the failure surface in  $U$ -space, which corresponds to the closest point of the failure surface to the origin (see Figure 3). The radius from the origin to the design point (the reliability index) is denoted  $\beta_F$ . Finally, the reliability index is used to estimate the structure’s probability of failure by assuming that the failure surface is linear at the design point, such that

$$\Phi(\beta_F) = 1 - \alpha, \quad (1)$$

where  $\Phi$  is the cumulative distribution function (CDF) of the standard univariate normal distribution.

In the IFORM approach, the location of the failure surface and design point are not known. Instead, the desired reliability index,  $\beta_F$ , is specified and the IFORM contour in  $U$ -space is defined as the set of points at radius  $\beta_F$ . The environmental contour in the original space is then obtained by applying the inverse Rosenblatt transformation to the contour in  $U$ -space.

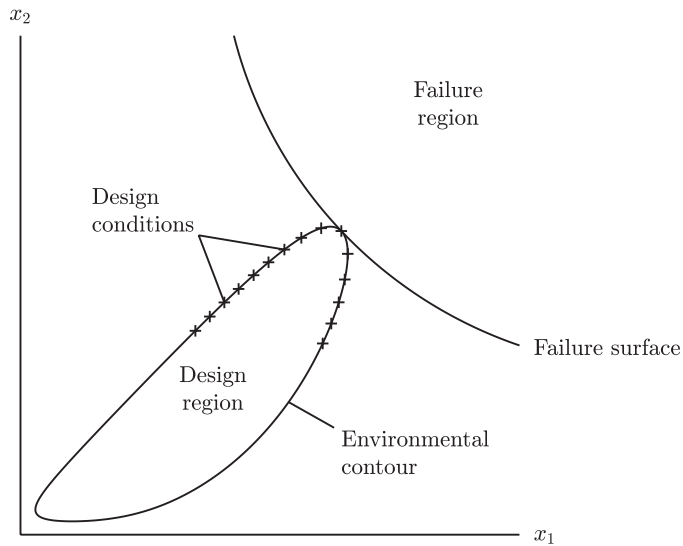


Figure 1: Illustration of terminology.

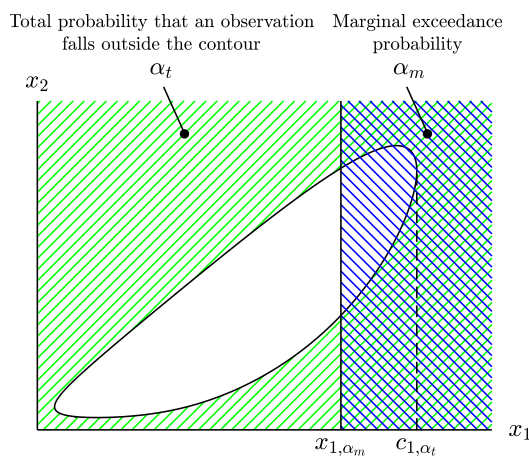


Figure 2: An environmental contour with its associated probabilities and return values.

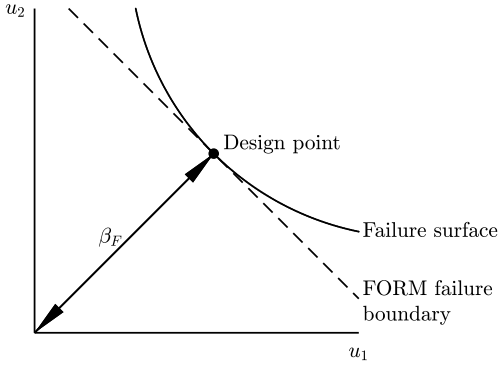


Figure 3: Illustration of FORM approximation to failure surface.

An illustration of the definition of the IFORM contour in 1D and 2D is shown in Figure 4 (a) and (b). Although contours are defined for two or more dimensions, the definition is still valid in 1D and serves to illustrate how the maximum value along the contour is related to the marginal return value. It is clear that the maximum value of each variable along an IFORM contour at probability  $\alpha$ , has marginal exceedance probability  $\alpha$ . Or in the notation defined above,  $Q(c_{j,\alpha}) = \alpha$ . Exceedances in the IFORM method can be thought of as marginal exceedances under a rotation of the axes.

### 2.2. Inverse second-order reliability method (ISORM)

The IFORM approximation is conservative when the failure surface is convex, but is not conservative if the failure surface is concave. Chai and Leira [8] proposed a second-order approximation to the failure surface which is always conservative. In the ISORM method the failure surface is assumed to enclose a circle in  $U$ -space. The radius  $\beta_{Sn}$ , is defined so that the probability that an observation falls outside the circular region is  $\alpha$ . Chai and Leira noted that since the sum of  $n$  independent standard normal variables follows a Chi-squared distribution on  $n$  degrees of freedom,  $\chi_n^2$ , the radius  $\beta_{Sn}$  can be written as:

$$\chi_n^2(\beta_{Sn}^2) = 1 - \alpha. \quad (2)$$

In the ISORM definition, the radius,  $\beta_{Sn}$ , is a function of both the exceedance probability  $\alpha$  and the number of dimensions,  $n$ . As with the IFORM contour, the ISORM contour in the original space is obtained by applying the inverse Rosenblatt transformation to the contour in  $U$ -space. An illustration of the definition of ISORM contours in 1D and 2D is shown in Figure 4 (c) and (d).

### 2.3. Direct sampling method (DS)

An alternative to the IFORM method was proposed by Huseby *et al.* [7]. Instead of applying the Rosenblatt transformation and defining the contour in  $U$ -space, the contour is defined in the original space in a similar way, with the failure surface in the original space assumed to be linear.

In 2D, the contours are constructed as follows. For a given angle  $\theta$ , the halfspace perpendicular to the line at angle  $\theta$  to the origin is found which contains probability  $\alpha$  (see Figure 4(f)). A finite number of angles are selected and contours are defined as the intersection of the lines bounding each halfspace. Huseby *et al.* proposed that the location of the halfspace at each angle could be estimated by Monte Carlo simulation under the joint distribution and projection of the variables on to the line at angle  $\theta$  to the origin:  $y = x_1 \cos \theta + x_2 \sin \theta$ . The distance of the halfspace from the origin is then found as the empirical quantile of  $y$  at exceedance probability  $\alpha$ .

The method can be interpreted as a rotation of the axes and calculation of a marginal exceedance probability on the rotated axes (this is also true of the IFORM method in  $U$ -space). The use of Monte Carlo simulation to estimate the marginal exceedances avoids numerical issues with integrating the joint distribution and allows the method to be easily extended into higher dimensions.

We see that, by definition, the DS contour passes through points with marginal exceedance probability  $\alpha$ . Since DS contours are defined as the intersection of straight line segments which describe exceedances at a given angle, the resulting contours are always convex, regardless of the shape of the joint distribution.

### 2.4. Highest density region method (HD)

Highest density (HD) contours can be thought of as the  $X$ -space analogue of ISORM contours in  $U$ -space, in the same way that DS contours are  $X$ -space analogues of IFORM contours  $U$ -space. HD contours were proposed as a conservative environmental contour that does not assume a convex failure surface [9]. They are defined based on highest density regions, a statistical concept used in a diverse range of contexts (see, for example, [33]). A highest

density region,  $R$ , is the smallest possible region in the variable space that contains a given probability content. Mathematically, it can be expressed as the set of all  $\mathbf{x}$  whose probability density is greater than a threshold  $f_c$ :

$$R(f_c) = \{\mathbf{x} \in \mathbb{R}^n : f(\mathbf{x}) \geq f_c\}, \quad (3)$$

where  $f(\mathbf{x})$  is the joint density function and  $f_c$  is chosen as the largest threshold that yields a region, which contains a probability of at least  $1 - \alpha$ , that is

$$f_c = \underset{f \in [0, \infty)}{\operatorname{argmax}} \Pr(\mathbf{X} \in R(f)) \geq 1 - \alpha. \quad (4)$$

Then, the  $\alpha$ -exceedance highest density contour is defined as the set  $C(\alpha) \subset R(c_\alpha)$  that contains exactly the environmental states at which the probability density equals  $f_c$ :

$$C(\alpha) = \{\mathbf{x} \in \mathbb{R}^n : f(\mathbf{x}) = f_c\}. \quad (5)$$

### 3. Marginal probabilities associated with ISORM contours

The marginal exceedance probability associated with an ISORM contour in  $n$  dimensions can be calculated as follows. For a given contour exceedance probability,  $\alpha_c$ , the radius,  $\beta_{Sn}$ , of the ISORM contour in  $U$ -space is given by (2). The marginal exceedance probability,  $\alpha_m$ , associated with  $\beta_{Sn}$  is then given by

$$\alpha_m = 1 - \Phi(\beta_{Sn}). \quad (6)$$

As the exceedance probability is invariant under the Rosenblatt transformation,  $\alpha_m$  is the marginal exceedance probability of the largest value along the contour in any particular dimension,  $c_{\alpha_c}$ . As  $\alpha_c = \alpha_t$  for ISORM contours, there is a fixed relationship between the probability of an observation falling outside the contour,  $\alpha_t$ , and the marginal exceedance probability of the highest point along the contour  $\alpha_m$ . Figure 5 shows the ratio  $\alpha_t/\alpha_m$  against  $\alpha_t$  for  $n = 1, \dots, 5$ . For a one dimensional ISORM contour, the exceedance probability is split evenly between the upper and lower tails of the distribution, so the contour has an non-exceedance probability of  $\alpha_t/2$  in the lower tail and an exceedance probability of  $\alpha_t/2$  in the upper tail. Consequently, in 1D we have  $\alpha_t/\alpha_m = 2$ . For higher dimensions, the marginal exceedance probability associated with the maximum point on the  $\alpha_t$ -ISORM contour, increases with both  $\alpha_t$  and the number of dimensions. In two dimensions, the marginal exceedance probability associated with an ISORM contour at exceedance probability  $\alpha_t = 10^{-3}$  is 10 times lower than the total exceedance probability, and for a 4-dimensional contour the marginal exceedance probability associated with  $\alpha_t = 10^{-3}$  is 100 times lower.

The ratio  $\alpha_t/\alpha_m$  is the ratio of the return period of  $c_{\alpha_t}$  to the contour return period. For example, if sea states are observed at 3 hour intervals, the 50-year contour corresponds to an exceedance probability of  $\alpha_t = 1/(50 \times 362.25 \times 24/3) = 6.84 \times 10^{-6}$ . So the 50-year 2D ISORM contour passes through points with marginal return periods of 635 years. Similarly, the 50-year 4D ISORM contour passes through points with marginal return periods of 10,950 years. Or to put it another way, since IFORM contours are defined in terms of marginal probabilities, we can say that for 3-hour observations of 2 variables the 50-year ISORM is equivalent to the 635-year IFORM contour and for 4 variables the 50-year ISORM contour is equivalent to the 10,950-year IFORM contour.

The difference between  $c_{\alpha_t}$  and  $x_{\alpha_t}$  depends on the shape of the tail of the distribution. For long-tailed distributions a small change in return period results in a large change in the return value, whereas for short-tailed distributions a large change in return-period will only result in a small change in return value. An example is given here assuming that the variable of interest follows a Weibull distribution, with CDF

$$F(x) = 1 - \exp\left(-\left(\frac{x - \gamma}{\lambda}\right)^k\right). \quad (7)$$

Figure 6 shows the Weibull distribution for cases with location parameter  $\gamma = 0$ , scale parameter  $\lambda = 1$  and various shape parameters  $k$ . When  $k = 1$  the distribution has an exponential tail. As  $k$  increases the upper tail becomes shorter. The ratio between the highest point on the 50-year ISORM contour and the 50-year marginal return value (denoted  $c_{50}$  and  $x_{50}$ , for brevity) is shown in Figure 7 as a function of the Weibull shape parameter,  $k$  for contours in  $n = 1, \dots, 5$  dimensions. Here we assume a location parameter  $\gamma = 0$  (the ratio  $c_{50}/x_{50}$  is invariant to scale,  $\lambda$ ) and assume observations at 3-hour intervals as above. The ratio  $c_{50}/x_{50}$  decreases as the Weibull shape parameter increases and the upper tail becomes shorter. For a 2D contour  $c_{50}$  is 21% larger than  $x_{50}$  when  $k = 1$  and 10% larger when  $k = 2$ . For a 4D contour  $c_{50}$  is 45% larger than  $x_{50}$  when  $k = 1$  and 20% larger when  $k = 2$ . These differences can potentially have a large impact on the strength requirements for a structure, so the decision between the use of an ISORM contour over an IFORM or DS contour needs to be carefully justified. Some examples where each type may appropriate are presented in Section 7.

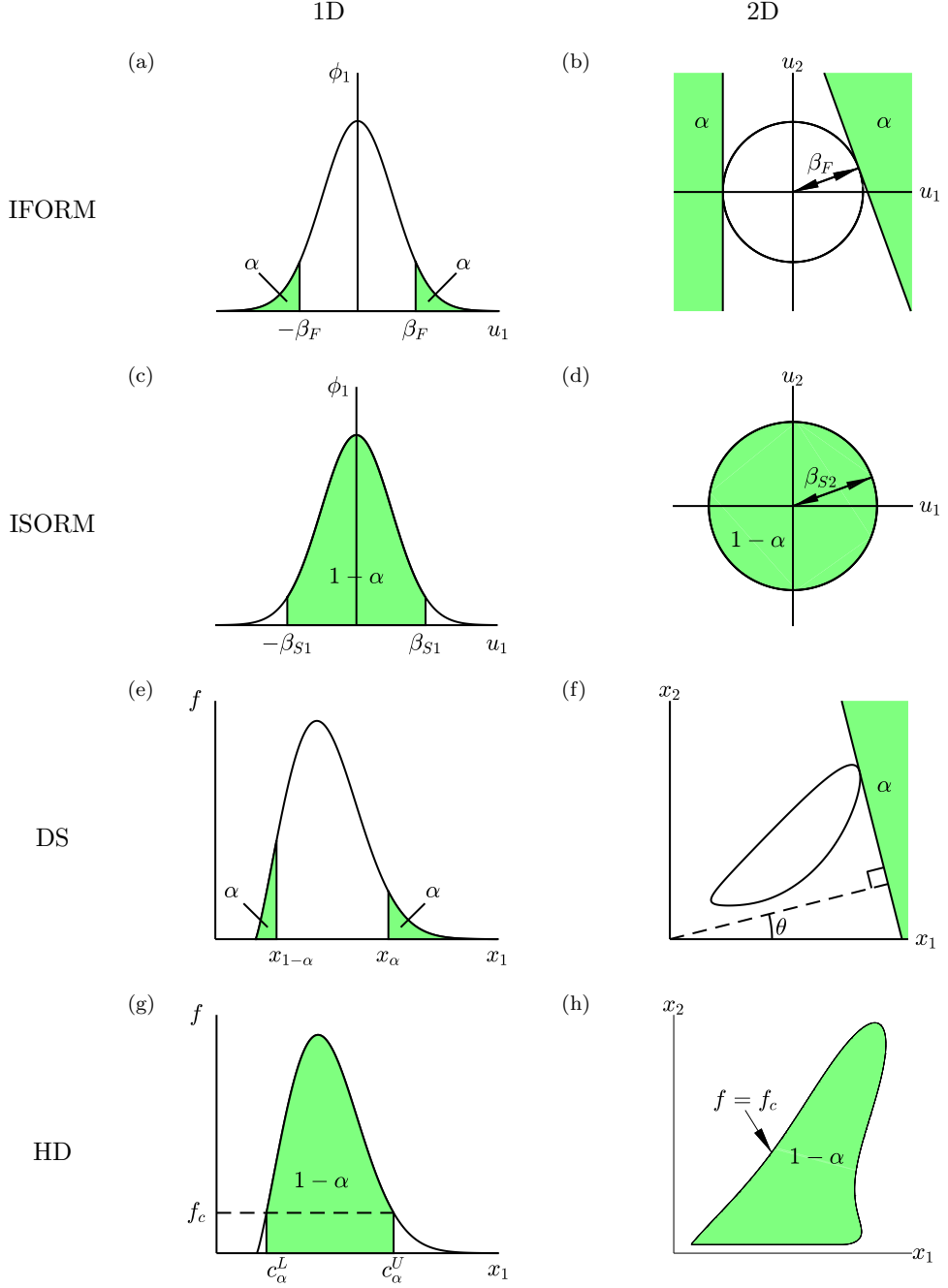


Figure 4: Illustration of definitions of IFORM, ISORM, direct sampling (DS) and highest density (HD) contours in 1D and 2D.

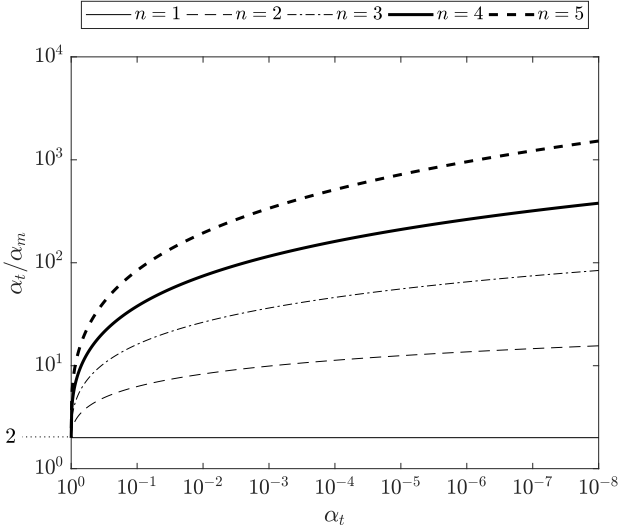


Figure 5: Ratio of total exceedance probability,  $\alpha_t$ , to marginal exceedance probability of highest value on contour,  $\alpha_m = Q(c_{\alpha_t})$ , against  $\alpha_t$  for ISORM contours in  $n = 1, \dots, 5$  dimensions.

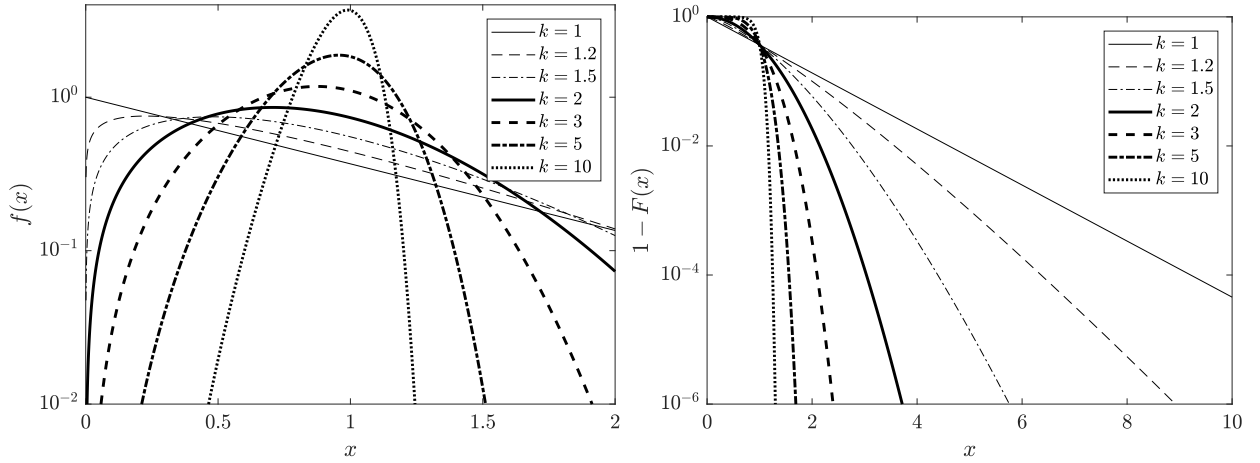


Figure 6: Left: PDF of the Weibull distribution. Right: Upper tail of the Weibull distribution function. Both plots for location parameter  $\gamma = 0$ , scale parameter  $\lambda = 1$  and various shape parameters  $k$ .

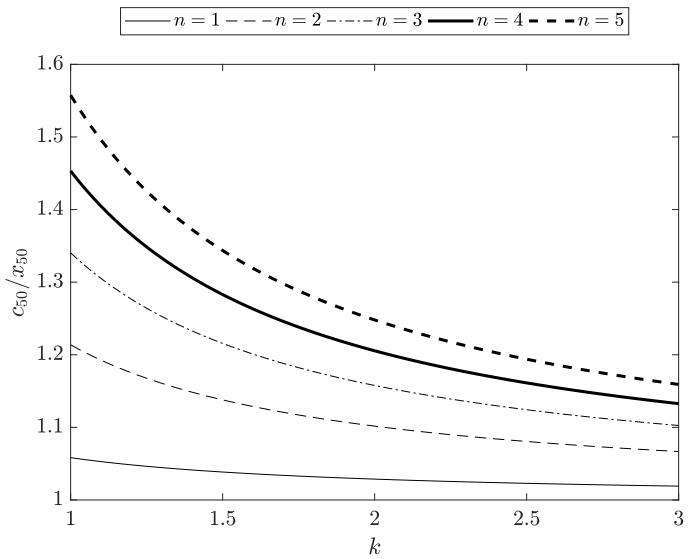


Figure 7: Ratio of the highest point on a 50-year ISORM contour,  $c_{50}$ , to the 50-year marginal return value,  $x_{50}$ , assuming a marginal Weibull distribution with location parameter  $\gamma = 0$  and shape parameter  $k$ . Results shown for ISORM contours in  $n = 1, \dots, 5$  dimensions.

#### 4. Marginal probabilities associated with HD contours

HD contours are based on the same notion of exceedance as ISORM contours (i.e. an exceedance is a point anywhere outside the contour,  $\alpha_c = \alpha_t$ ), so we may expect a similar relationship between the total exceedance probability and the marginal exceedance probabilities of  $c_{j,\alpha_t}$ . For HD contours in any number of dimensions we have, by definition,  $c_{j,\alpha_t} \geq x_{j,\alpha_t}$ , since it is not possible for a region of parameter space bounded by  $x_{j,\alpha_t}$  in one dimension to contain a probability greater than  $\alpha_t$ .

However, as the HD contour is defined as an isodensity contour in the original parameter space, the relationship between  $Q(c_{j,\alpha_t})$  and  $\alpha_t$  is dependent on the shape of the density function. Consider the 1D case shown in Figure 4 (g). In the example shown it is clear that  $F(c_\alpha^L) < Q(c_\alpha^U)$  (where  $c_\alpha^L$  and  $c_\alpha^U$  are the lower and upper bounds of the contour respectively). In general we have  $F(c_\alpha^L) < Q(c_\alpha^U)$  when the lower tail is steeper than the upper tail,  $F(c_\alpha^L) > Q(c_\alpha^U)$  when the upper tail is steeper than the lower tail and  $F(c_\alpha^L) = Q(c_\alpha^U)$  when the distribution is symmetric. So the non-exceedance probability of the contour lower bound and exceedance probability of the contour upper bound are not in fixed relation to the contour exceedance probability.

Consider the hypothetical cases where the probability density function (PDF) has a triangular shape, shown in Figure 8. In the extreme case, where the lower tail has a vertical gradient, the  $\alpha$ -exceedance probability HD contour has zero non-exceedance probability in the lower tail and exceedance probability  $\alpha$  in the upper tail, so that  $c_\alpha = x_\alpha$  (i.e. the upper bound of the  $\alpha$ -exceedance contour is equal to the  $\alpha$ -exceedance marginal quantile). In the case that the PDF is symmetric, the exceedance probability is split evenly between the lower and upper tails so that  $c_\alpha = x_{\alpha/2}$  (i.e. the upper bound of the  $\alpha$ -exceedance contour is equal to the marginal quantile at exceedance probability  $\alpha/2$ ). In the other extreme case, where the upper tail has a vertical gradient and an upper end point at  $x_m$ , the exceedance probability of the upper bound of the HD contour is zero and  $c_\alpha = x_m$  (i.e. the upper bound of the contour is the upper end point of the distribution).

These examples are unrealistic, but serve to illustrate the sensitivity of the minimum and maximum points on the contour to the shape of the density function. Now consider a more realistic 1D example, where the random variable  $X_1$  follows a Weibull distribution. The PDF of the Weibull distribution is

$$f(x) = \frac{k}{\lambda} \left( \frac{x - \gamma}{\lambda} \right)^{k-1} \exp \left[ - \left( \frac{x - \gamma}{\lambda} \right)^k \right]. \quad (8)$$

When  $k = 0$  the PDF has a vertical gradient in the lower tail and a long upper tail (see Fig. 6). As  $k$  increases, the gradient of the lower tail decreases and the gradient of the upper tail increases. As  $k \rightarrow \infty$  the PDF converges towards a Dirac delta distribution centered at  $x = \lambda$ . However, for large finite  $k$  the gradient of the lower tail is less than the gradient of the upper tail.

The effect that the shape of the PDF has on the upper bound of the contour is assessed as follows. For a given contour exceedance probability  $\alpha_c$ , the  $\alpha_c$ -exceedance HD contour is calculated and the upper bound of the contour  $c_{\alpha_t}$  is found. The ratio  $c_{\alpha_t}/x_{\alpha_t}$  of the contour upper bound to the marginal quantile at exceedance probability  $\alpha_t$  is shown in Figure 9 as a function of Weibull shape parameter  $k$  for various contour exceedance probabilities  $\alpha_t$ . When  $k = 1$  we have  $c_{\alpha_t} = x_{\alpha_t}$  at all exceedance probabilities, since the lower tail of the PDF has a vertical gradient. As  $k$  increases the ratio  $c_{\alpha_t}/x_{\alpha_t}$  increases as the gradients in the upper and lower tail change. The ratio  $c_{\alpha_t}/x_{\alpha_t}$  is dependent on the exceedance probability, since the gradients in the tails are not constant, with  $c_{\alpha_t} \rightarrow x_{\alpha_t}$  as  $\alpha_t \rightarrow 0$ . As  $k$  increases and the upper tail becomes shorter than the lower tail,  $c_{\alpha_t} \rightarrow x_{\alpha_t}$  since the value of  $x_{\alpha_t}$  becomes less sensitive to the exceedance probability  $\alpha_t$ .

The ratio of the contour exceedance probability to the exceedance probability of the largest point on the contour,  $\alpha_t/Q(c_{\alpha_t})$ , is also shown in Figure 9. In this case the ratio increases monotonically with  $k$ . For smaller values of  $k$  the ratio  $\alpha_t/Q(c_{\alpha_t})$  is larger for larger values of  $\alpha_t$ , but at higher values of  $\alpha_t$  the trend is reversed. Although  $\alpha_t/Q(c_{\alpha_t})$  can be large for large  $k$ , the difference between  $c_{\alpha_t}$  and  $x_{\alpha_t}$  is small since the distribution has a steep gradient in the upper tail.

In these examples we see that the relationship between the highest point on the HD contour and the marginal quantile at the same exceedance probability is relatively insensitive to the shape of the distribution, despite large differences in the exceedance probability.

In two dimensions the relationship between the marginal exceedance probability of the maximum point along a contour and contour exceedance probability is slightly different. Consider the following simple cases where  $X_1$  follows a Weibull distribution with  $\gamma = 0$ ,  $\lambda = 1$  and  $k = 1$  and  $X_2$  is independent of  $X_1$ , and is either uniformly distributed over  $[-3, 3]$  or follows a standard normal distribution. The joint PDF for the two cases are illustrated in Figure 10, together with the HD contour at  $\alpha_t = 0.1$  and the marginal quantile  $x_{1,\alpha_t}$ . As the Weibull shape parameter is 1, the joint PDF has a vertical gradient at  $x_1 = 0$ . In the case where  $X_2$  is uniformly distributed the  $\alpha_t$ -exceedance HD contour is simply a line at the marginal quantile  $x_{1,\alpha_t}$ . However, when the joint density contours are no longer straight lines parallel to the  $X_2$  axis, the highest value of  $x_1$  along the  $\alpha_c$ -exceedance HD contour will be greater than  $x_{1,\alpha_t}$ , since the region  $X_1 < x_{1,\alpha_t}$  is no longer the highest density region containing a probability  $1 - \alpha_t$ . So in two dimensions, the criteria that one variable has a vertical gradient in the lower tail of the PDF is no longer sufficient to ensure that  $c_{\alpha_t} = x_{\alpha_t}$  and in general we will have  $c_{\alpha_t} > x_{\alpha_t}$ .

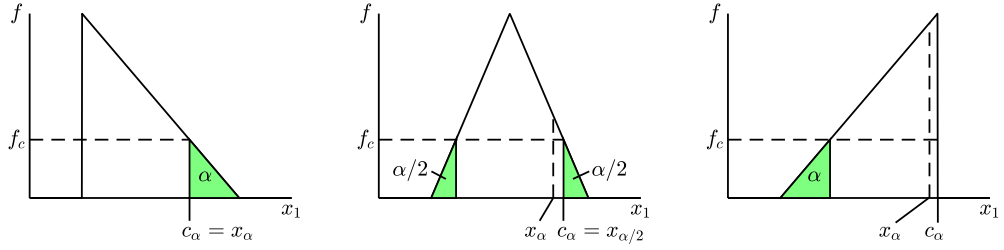


Figure 8: Examples of marginal and contour exceedance levels for HD method applied to 1D triangular PDFs.

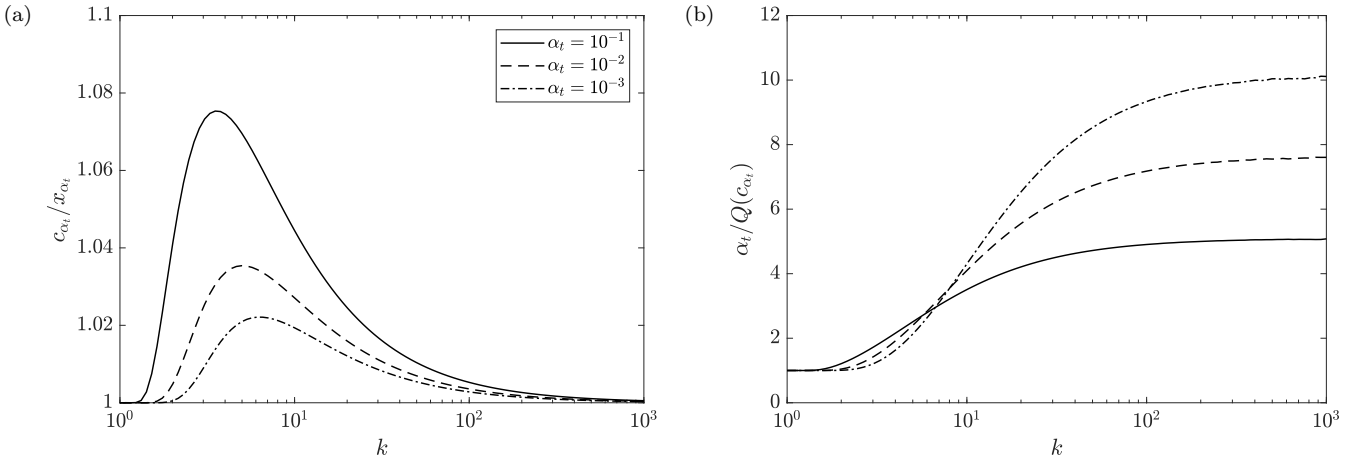


Figure 9: (a) Ratio  $c_{\alpha_t}/x_{\alpha_t}$  for a 1D HD contour. (b) Ratio of contour exceedance probability to marginal exceedance probability of highest point along contour. Both ratios shown as a function of Weibull shape parameter,  $k$  for various total exceedance probabilities  $\alpha_t$ .

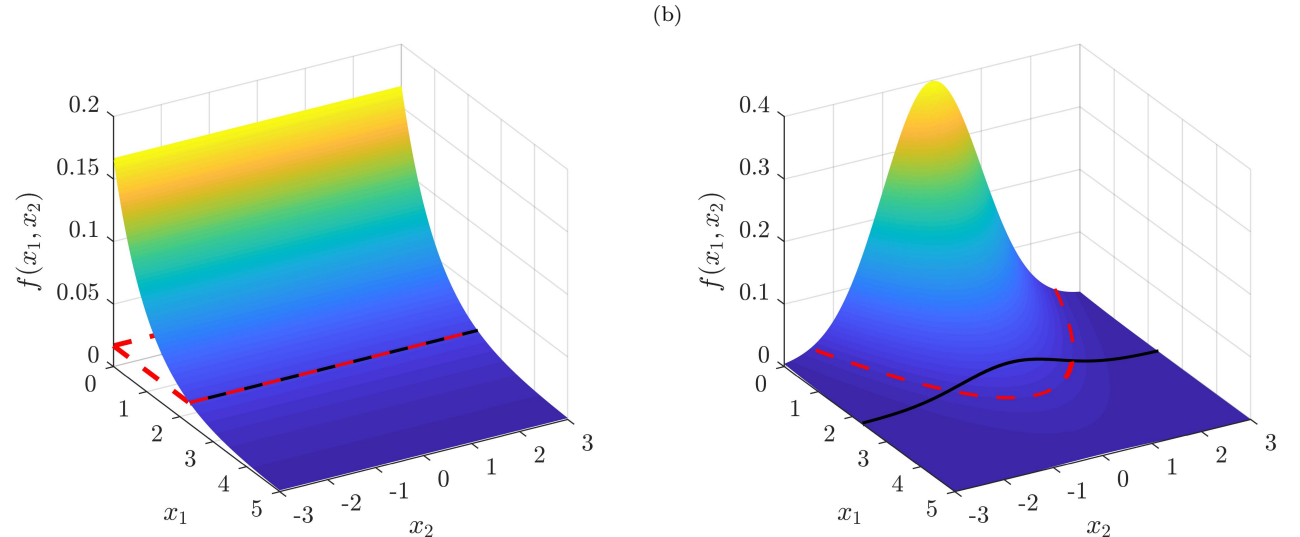


Figure 10: (a) Joint PDF where  $X_1$  is Weibull distributed with shape parameter  $k = 1$  and  $X_2$  is independent and uniformly distributed. (b) Joint PDF where  $X_1$  is Weibull distributed with shape parameter  $k = 1$  and  $X_2$  is independent and normally distributed. Black lines indicate marginal quantile of  $X_1$  at  $\alpha = 0.1$ . Red dashed lines indicate HD contour at  $\alpha = 0.1$ . In case (a) the HD contour coincides with the marginal quantile.

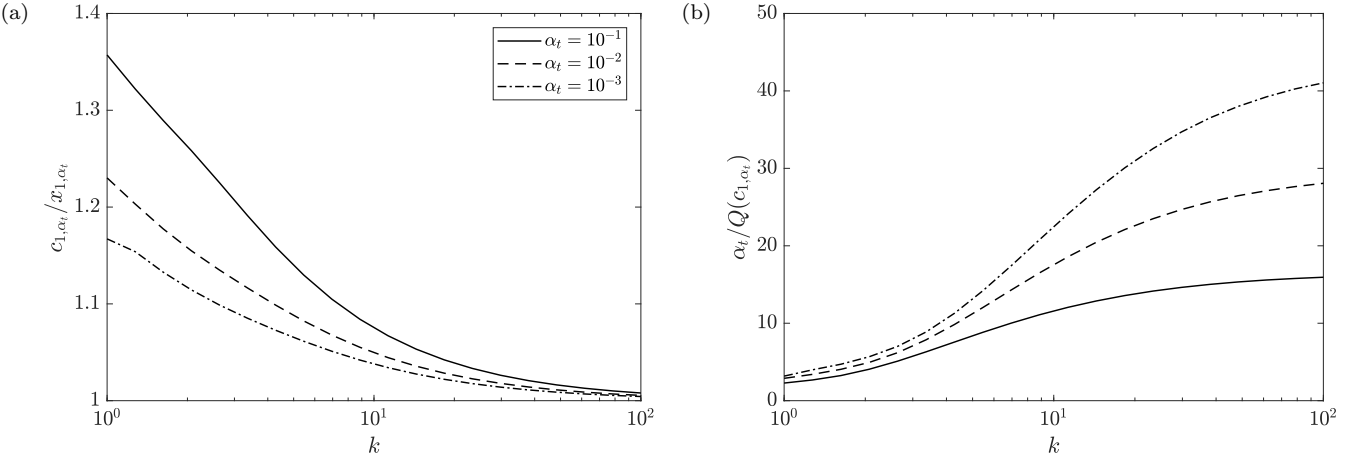


Figure 11: (a) Ratio  $c_{1,\alpha_t}/x_{1,\alpha_t}$  for a 2D HD contour, where  $X_1$  is Weibull distributed and  $X_2$  is independent and normally distributed. (b) Ratio of contour exceedance probability to marginal exceedance probability of highest point along contour. Both ratios shown as a function of Weibull shape parameter,  $k$  for various total exceedance probabilities  $\alpha_t$ .

The effect of the Weibull shape parameter on the ratios  $c_{1,\alpha_t}/x_{1,\alpha_t}$  and  $\alpha_t/Q(c_{1,\alpha_t})$  is illustrated in Figure 11 for the case where  $X_1$  is Weibull distributed and  $X_2$  is independent of  $X_1$  and follows a standard normal distribution. In contrast to the 1D case, the ratio  $c_{1,\alpha_t}/x_{1,\alpha_t}$  for the 2D contour is monotonically decreasing with both the shape parameter  $k$  and contour exceedance probability  $\alpha_t$ . As noted above, when  $k = 1$ , we have  $c_{1,\alpha_t} > x_{1,\alpha_t}$ . As  $k$  increases and the gradient of the upper tail increases and the gradient of the lower tail decreases, the position of the HD contour is shifted towards higher values of  $X_1$  and the upper bound of the contour tends toward  $x_{1,\alpha_t}$ . In general, the differences between the 1D case and 2D case will be dependent on the shape of the joint distribution. In the case that  $X_2$  is uniformly distributed, the 2D case is identical to the 1D case (in terms of the upper and lower bounds of the contour). As the distribution of  $X_2$  moves away from being uniform, the differences between the 1D case and 2D case will increase.

To illustrate the relationship between marginal and contour exceedance probabilities and quantiles in a more realistic case, we use a sea state model that has been used in several previous studies on environmental contours (e.g. [34, 9, 8, 7]). The model describes the bivariate distribution of significant wave height,  $H_s$ , and zero-up-crossing period,  $T_z$ . The joint density function is written as

$$f_{H_s, T_z}(h_s, t_z) = f_{H_s}(h_s)f_{T_z|H_s}(t_z|h_s), \quad (9)$$

where  $H_s$  is assumed to follow a translated Weibull distribution (8) and  $T_z$  follows a log-normal distribution conditional on  $H_s$ :

$$f_{T_z|H_s}(t_z|h_s) = \frac{1}{t_z\sigma\sqrt{2\pi}} \exp\left[\frac{-(\ln t_z - \mu)^2}{2\sigma^2}\right]. \quad (10)$$

The Weibull distribution's parameters are  $\lambda = 2.776$ ,  $k = 1.471$  and  $\gamma = 0.8888$  while the conditionality of  $T_z|H_s$  is modelled with two dependence functions:

$$\begin{aligned} \mu &= 0.1 + 1.489h_s^{0.1901}, \\ \sigma &= 0.04 + 0.1748 \exp(-0.2243h_s). \end{aligned} \quad (11)$$

Figure 12(a) shows the computed HD contours at exceedance probabilities  $\alpha_t \in [10^{-7}, 10^{-1}]$ . The influence of the Weibull shape parameter on the 2D contours was also investigated. Figure 12(b) shows the HD contours at an exceedance probability of  $\alpha_t = 10^{-5}$  for distributions with various Weibull shape parameters (all other parameters of the joint distribution have been left unchanged).

For comparison with the 1D case, we will consider the maximum value of  $H_s$  along the HD contour, as the marginal distribution of  $H_s$  is Weibull. Figure 13(a) shows the ratio  $c_{\alpha_t}/x_{\alpha_t}$ , of the maximum value of  $H_s$  along the contour to the marginal value of  $H_s$  at the same exceedance probability. The ratio is shown as a function of the contour exceedance probability  $\alpha_t$  for values of  $k$  between 1 and 3. As in the 1D case, the ratio is larger at higher exceedance probabilities. The variation of  $c_{\alpha_t}/x_{\alpha_t}$  is similar to the simple case above, where  $X_2$  is independent and normally distributed, with the ratio decreasing as  $k$  increases and the marginal distribution of  $X_1$  has a steeper gradient in the upper tail. At an exceedance probability of  $\alpha_t = 10^{-6}$  the HD contour maximum  $H_s$  is approximately 5% larger than the marginal quantile when  $k = 3$  and approximately 10% larger when  $k = 1$ . However, in the 1D case we had  $c_{\alpha_t} = x_{\alpha_t}$  when  $k = 1$ , whereas in 2D  $c_{\alpha_t} > x_{\alpha_t}$  when  $k = 1$ , despite the gradient of lower tail of the distribution being vertical at the lower end point of the distribution.

Figure 13(b) shows the ratio  $\alpha_t/Q(c_{\alpha_t})$ , of the total exceedance probability to marginal exceedance probability of highest  $H_s$  value along contour. As in the 1D case, the ratio of probabilities increases as the exceedance probability

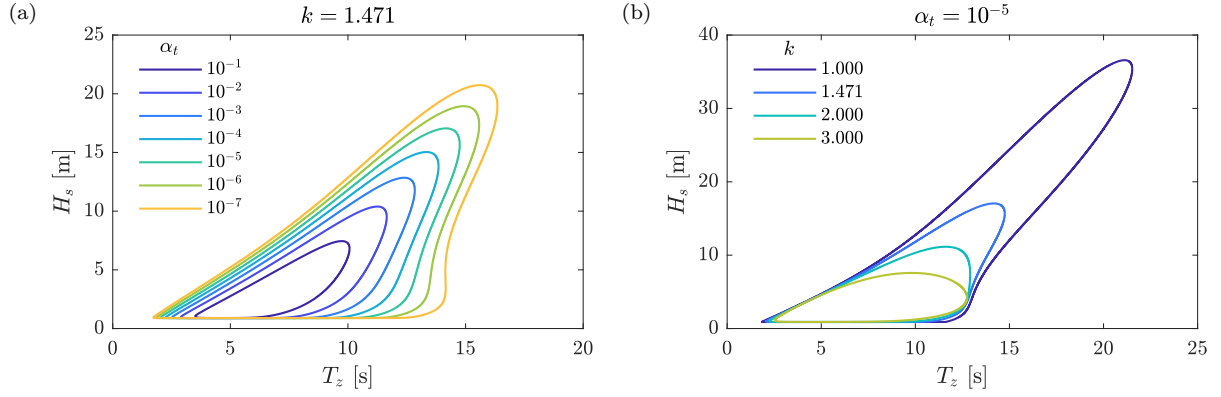


Figure 12: (a) HD contours of joint density function described in (9)-(11) at various contour exceedance probabilities  $\alpha_t$ . (b) HD contours at exceedance probability  $\alpha_t = 10^{-5}$  for same joint distribution shown in (a), but with various values of Weibull shape parameter  $k$  (all other parameters held constant).

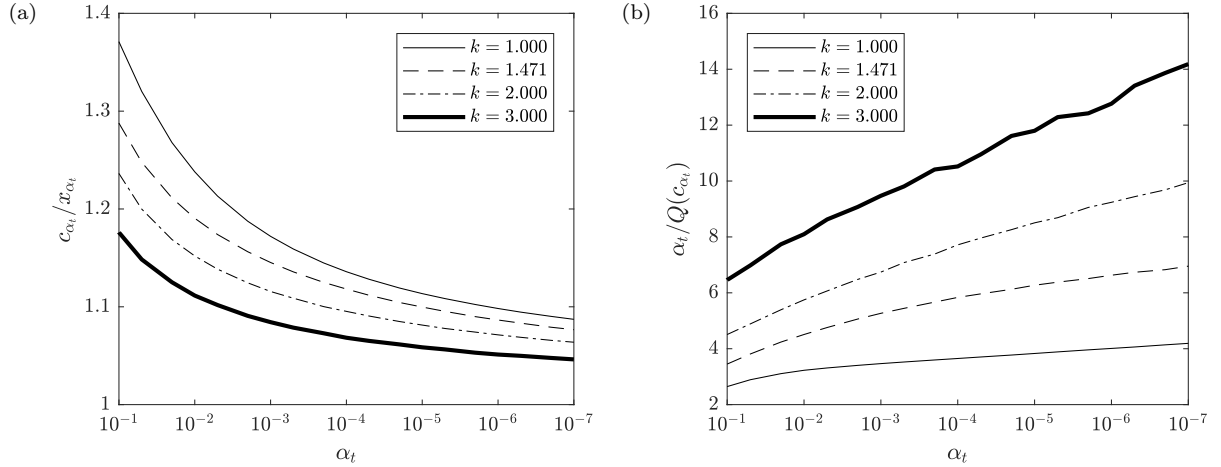


Figure 13: (a) Ratio of  $H_s$  return values for HD contours of joint distribution shown in previous figure. (b) Ratio of contour exceedance probability to marginal exceedance probability of highest  $H_s$  value along contour.

decreases and also as the tail becomes shorter. For a total exceedance probability of  $10^{-6}$  the marginal exceedance probability of the highest  $H_s$  along the contour is approximately 4 times lower when  $k = 1$  and approximately 13 times lower when  $k = 3$ .

## 5. Total probability outside IFORM contours

We now consider the complementary problem of calculating the probability that an observation falls outside a contour. For an IFORM contour defined at marginal exceedance probability  $\alpha_m$ , the radius of the contour in  $U$ -space,  $\beta_F$ , is given by (1). The total probability outside the contour,  $\alpha_t$ , is then given by

$$\alpha_t = 1 - \chi_n^2(\beta_F^2). \quad (12)$$

The relationship between  $\alpha_m$  and  $\alpha_t$  derived here is the same as in Section 3. However, for ease of interpretation, the ratio  $\alpha_t/\alpha_m$  is plotted against  $\alpha_m$  in Figure 14 for  $n = 1, \dots, 5$ . Note that the lowest possible marginal exceedance probability for an IFORM contour is 0.5 and in this case the corresponding total exceedance probability is 1. Therefore all the lines in Figure 14 converge at  $\alpha_m = 0.5$ ,  $\alpha_t/\alpha_m = 2$ . In two dimensions the ratio  $\alpha_t/\alpha_m = O(10)$  for  $\alpha_m \leq 10^{-3}$ . This means that the probability of observing an exceedance anywhere outside the contour is approximately 10 times higher than the probability of observing an exceedance in any particular half-plane tangential to the contour (i.e. a marginal exceedance at probability  $\alpha_m$  under some rotation of the axes). For a given marginal exceedance probability, the probability of observing an exceedance anywhere outside the contour increases with the number of dimensions, since there are more combinations of variables that are outside the contour. For example, in 4D, for an IFORM contour defined at a marginal exceedance probability  $\alpha_m = 10^{-5}$  the total exceedance probability is approximately 100 times higher.

## 6. Total probability outside DS contours

The probability that an observation falls outside an DS contour was investigated using numerical simulation. The joint distribution of  $H_s$  and  $T_z$  used in Section 4 was used to simulate a sample of  $10^8$  observations. DS contours

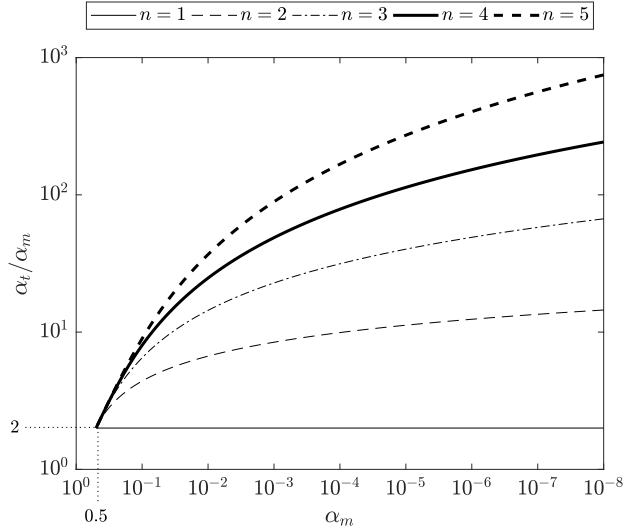


Figure 14: Ratio of total exceedance probability,  $\alpha_t$ , to marginal exceedance probability  $\alpha_m$ , against  $\alpha_m$  for IFORM contours defined at exceedance probability  $\alpha_m$  in  $n = 1, \dots, 5$  dimensions.

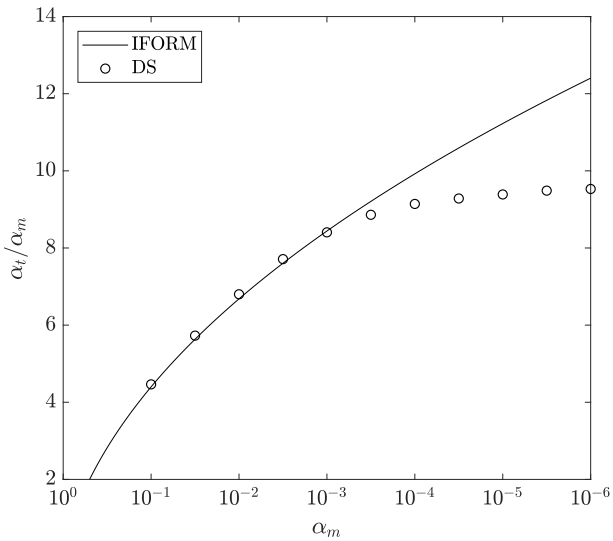


Figure 15: Comparison of ratio of total exceedance probability,  $\alpha_t$ , to marginal exceedance probability  $\alpha_m$ , against  $\alpha_m$  for DS and IFORM contours in 2 dimensions. Results for the DS contour are based on the joint distribution given in (9).

were calculated with marginal exceedance probabilities in the range  $\alpha_m \in [10^{-6}, 10^{-1}]$ . For each marginal exceedance probability, the number of points falling outside the contour was counted to obtain an empirical estimate of  $\alpha_t$ . Figure 15 shows the ratio  $\alpha_t/\alpha_m$  against  $\alpha_m$  for the DS contour and an IFORM contour. The ratio of total to marginal exceedance probability for the DS contour is almost identical to that for an IFORM contour for exceedance probabilities greater than  $10^{-3}$ , but the ratio for the DS contour is slightly lower than that for the IFORM contour at lower exceedance probabilities.

The IFORM contour can be thought of as a special case of the DS contour, when the data are independent normal variables. In this special case, the ratio  $\alpha_t/\alpha_m$  would be identical for both DS and IFORM contours at all exceedance probabilities. In general, we would expect DS and IFORM contours to be very closely matched when the isodensity contours of the joint distribution are convex. The difference in the ratio at low exceedance probabilities shown in Figure 15 is likely to be related to the shape of the joint distribution, which becomes concave at lower exceedance probabilities (see Figure 12(a)). As the DS contour is convex and the IFORM contour is concave, this may cause some differences in the ratio  $\alpha_t/\alpha_m$ . In general, the relationship between the total probability outside the contour and the marginal exceedance probability is likely to be dependent on the shape of the joint distribution. However, as DS and IFORM contours are both defined in terms of marginal exceedances, the ratio  $\alpha_t/\alpha_m$  for DS contours is likely to be similar to that for IFORM contours in higher dimensions as well.

Method	50-year response	Sea state causing 50-year response ( $h_s, t_p$ )
IFORM contour	14.5	15.0 m, 17.6 s
DS contour	14.7	15.1 m, 17.7 s
ISORM contour	18.2	17.1 m, 18.8 s
HD contour	17.1	16.6 m, 18.4 s
All sea state approach	14.5	-

Table 1: Structural responses from different contour methods for a single degree of freedom system.

## 7. Implications for the design process

The previous sections showed that IFORM, DS, ISORM and HD contours that are calculated using the same  $\alpha$ -value can lead to significantly different design conditions. Further, the marginal return periods of the maximum values of each variable along different kinds of contours can easily deviate by a factor of 10. Thus, the type of contour used in the design process of a marine structure can have an important influence on the assumed environmental loads and consequently on the structure that is being designed. As, by definition, ISORM and HD contours are more conservative than IFORM and DS contours, it seems sensible to use these conservative contours only when they are required, that is, when the structure of interest has a non-convex failure surface. In a design project one does not know the exact shape of the failure surface beforehand, however, one can often anticipate its approximate shape. In the following we consider two simple examples, whose response characteristics are representative of wider classes of structural problems. In the first example we consider the response of a single degree of freedom system to sea states, where the use of IFORM or DS contours is more appropriate. In the second example we consider the specification of directional design conditions, where the use of ISORM or HD contours is more appropriate. To simplify the examples, it is assumed that the structural responses are deterministic so that it is not necessary to use inflation factors for the contours.

### 7.1. Example 1: Response of a single degree of freedom system to sea states

Consider the design process of a marine structure whose behaviour can be approximated as a single degree of freedom vibration system (see, for example, [3, Chapter 2]). This could be, for example, a vibrating tower [3, pp. 23] or a floating system [35]. Assume that a candidate design needs to be evaluated to check whether it fulfills a given reliability target. Suppose that failure is only allowed to occur with a return period of 50 years (or more seldom) such that a 50-year environmental contour is constructed to derive a set of design conditions.

We assume that the candidate design responds with the following deterministic response function, proposed in [2]:

$$r(h_s, t_p) = a \frac{h_s}{1 + b(t_p - t_{p0})^2} \quad (13)$$

where  $a = 2$ ,  $b = 0.007$  and  $t_{p0} = 30$  s. The response function peaks at a particular period  $t_{p0}$ , which could represent the Eigenfrequency of the system. In this example, the peak response occurs at a period, which is higher than the wave periods of typical sea states, which could represent the heave motions of a spar or surge motions of a tension leg platform [36]. As the response function peaks at a single  $t_p$  value, any response surface and consequently also the failure surface will be convex.

In this example, we assume that the joint distribution of  $h_s$  and  $t_p$  at the location of the structure is described by the model presented in Section 6, with a fixed relationship between  $t_p$  and  $t_z$  given by  $t_p = 1.2796t_z$ . The 50-year IFORM, ISORM, DS and HD contours for this environmental model are shown in Figure 16 and the position of the highest response along each contour is marked with a cross. The highest response along each contour is listed in Table 1 and ranges from 14.5 (IFORM contour) to 18.2 (ISORM contour).

The true long-term distribution can be calculated using the expression

$$F_R(x) = \iint_{r(h_s, t_p) \leq x} f_{Hs, Tp}(h_s, t_p) dt_p dh_s. \quad (14)$$

The true 50-year response for this example was calculated as 14.5. Thus, the computed IFORM and DS responses deviate less than 2% from the true 50-year response, whereas the responses from the HD and ISORM contours are 18% and 26% higher respectively than the true 50-year response.

Suppose that the structure has been optimized with respect to the design conditions that were derived from the 50-year DS contour such that a response that exceeds 15 represents failure. The resulting convex failure surface would almost touch the IFORM and DS contours, but the failure region would overlap with the ISORM and HD contours (Figure 17). Consequently, if ISORM or HD contours were used, the candidate design would need to be changed, either to reduce the response or increase the capacity.

In this example, the failure surface is convex and consequently the probability of failure is less than the DS contour's probability of exceedance,  $\alpha_M$ . Consequently, using the DS or IFORM contour would be a better choice than using an HD or ISORM contour as otherwise unnecessary conservatism would be introduced.

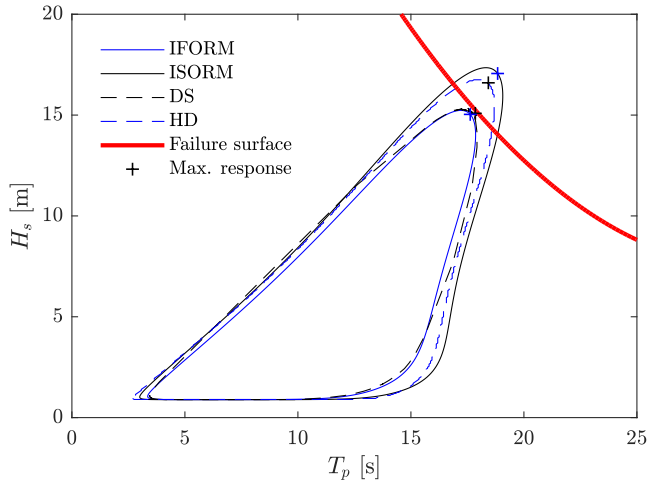


Figure 16: Design of a single degree of freedom system with a sea state environmental contour. The assumed response function peaks at the Eigenfrequency,  $t_{p0} = 30$  s. The failure surface would be acceptable if an IFORM or DS contour was used, but not acceptable if an HD or ISORM contour were used.

If the structure has multiple Eigenfrequencies, however, the failure surface will not be convex and it is not clear whether the exceedance probability of an DS or an IFORM contour,  $\alpha_M$ , is greater than the structure's probability of failure. In these cases, further analysis is required to ensure that the probability of failure is below the required value.

### 7.2. Example 2: Directional design conditions

In this example we consider the specification of directional design conditions for the design or assessment of a marine structure. In many locations, the severity of wave conditions exhibits a dependence on wave direction. Specifying the design wave height as a function of direction can allow the optimisation of an asymmetrical structure. Directional return values are often estimated in discrete directional sectors. However, it is becoming more common to estimate extreme value models where the model parameters vary smoothly with direction (e.g. [37, 38]). In these cases, environmental contours can be used to define directional design conditions.

In this example, we use a simple description of the joint distribution of  $H_s$  and wave direction,  $\Theta$ , based on the joint distribution of wind speed and direction given in [39] and studied further in [40]. The joint density function is written as a hierarchical model:

$$f_{\Theta, H_s}(\theta, h_s) = f_{\Theta}(\theta) f_{H_s|\Theta}(h_s|\theta). \quad (15)$$

The marginal distribution of wave direction is expressed as a mixture of von Mises distributions,

$$f_{\Theta}(\theta) = \sum_{i=1}^n w_i f_i(\theta), \quad (16)$$

where  $w_i \in [0, 1]$  are weights and  $\sum_{i=1}^n w_i = 1$ . The PDF of the von Mises distribution is

$$f_i(\theta) = \frac{\exp(\kappa_i \cos(\theta - \mu_i))}{2\pi I_0(\kappa_i)}, \quad (17)$$

where  $I_0$  is the zero-order modified Bessel function of the first kind,  $\kappa_i$  is a concentration factor and  $\mu_i$  is the location parameter. The model for  $H_s$  conditional on direction is a three-parameter Weibull distribution (8), with parameter dependence on direction given in terms of a Fourier series:

$$\lambda(\theta) = a_0 + \sum_{j=1}^m a_j \cos(j\theta) + b_j \sin(j\theta), \quad (18)$$

$$k(\theta) = c_0 + \sum_{j=1}^m c_j \cos(j\theta) + d_j \sin(j\theta). \quad (19)$$

The model presented in [39] uses  $m = 8$  harmonics for the Fourier series. In this example we assume the Weibull location parameter is constant at  $\gamma = 0.5$ . The other distribution parameters are defined in Tables 2 and 3.

To ensure that the environmental contours are continuous for  $\theta = 0$  and  $\theta = 2\pi$ , it is more straightforward to calculate environmental contours in terms of the  $x$  and  $y$  components of significant wave height, defined as

$$h_x = h_s \cos(\theta), \quad h_y = h_s \sin(\theta). \quad (20)$$

$j$	$w_j$	$\mu_j$	$\kappa_j$
1	0.21	2.10	0.74
2	0.79	5.54	13.11

Table 2: Parameters for distribution of wave direction.

$j$	$a_j$	$b_j$	$c_j$	$d_j$
0	1.875		1.910	
1	0.345	-0.140	0.240	-0.130
2	-0.210	-0.820	-0.080	-0.170
3	-0.160	-0.200	-0.010	-0.030
4	-0.265	0.095	-0.110	0.030
5	-0.090	0.110	0.0004	0.003
6	0.070	0.070	0.060	0.020
7	0.030	0.020	0.060	0.020
8	0.030	-0.015	0.004	-0.010

Table 3: Directional Fourier coefficients for conditional distribution of  $H_s$ .

The joint density function of  $h_x$  and  $h_y$  can then be written

$$f_{H_x, H_y}(h_x, h_y) = f_{\Theta, H_s}(\theta, h_s) \left| \frac{\partial (h_s \cos(\theta), h_s \sin(\theta))}{\partial (h_s, \theta)} \right|^{-1} = \frac{f_{\Theta, H_s}(\theta, h_s)}{h_s}. \quad (21)$$

Note that since the Weibull location parameter,  $\gamma$ , is greater than zero in this example, the transformed density function is non-singular at the origin since  $f_{\Theta, H_s}(\theta, 0) = 0$ . The 1-year IFORM, ISORM, DS and HD environmental contours are shown in Figure 17 (assuming that observations are at 3 hour intervals). As the isodensity contours of the joint distribution are close to convex in polar coordinates (or equivalently in  $(h_x, h_y)$  coordinates), the DS and IFORM contours are in close agreement, as are the HD and ISORM contours. The HD and ISORM contours give directional return values of  $H_s$  approximately 1 m larger than the DS and IFORM contours.

Suppose that a structure has a deterministic response dependent on  $H_s$  and direction only. If a structure is designed using the omnidirectional return value at exceedance probability  $\alpha$ , denoted  $h_\alpha$ , so that the failure surface is located at  $h_\alpha$  and is independent of direction, then the probability of failure will be equal to  $\alpha$ , by definition, since  $h_\alpha$  is the value of  $H_s$  that is exceeded with probability  $\alpha$ , independent of direction. If the structure is asymmetric, and designed so that the failure surface is located at a value greater than or equal to  $h_\alpha$  in each direction, then the probability of failure will be less than or equal to  $\alpha$ . So the use of omnidirectional criteria gives the target failure probability, but may lead to a less efficient design as the potential to optimise the design with respect to direction is not exploited.

Now suppose that an asymmetric structure is optimised based on directional extreme conditions from an environmental contour. For example, the stiffness of a fixed structure in a particular direction could be optimised with respect to direction or similarly the mooring response of a floating structure could be optimised to allow larger responses in directions where the wave conditions are less severe. The IFORM and DS contours at exceedance probability  $\alpha$  describe the return values of  $H_s$  conditional on direction, with exceedance probability  $\alpha$ . Forristall [41] noted that if a structure is designed based on directional return values at exceedance probability  $\alpha$  then the failure probability of the structure is greater than  $\alpha$ . Consider a hypothetical marine structure that is fully optimized to directional criteria, such that failure occurs immediately if the directional criteria is exceeded. In such a case we can see from the results in Sections 5 and 6 that if the directional criteria are specified based on IFORM or DS contours then the failure probability will be approximately 10 times higher than the exceedance probability of the contour. So for this application the use of IFORM or DS contours is not conservative.

In contrast, the ISORM and HD contours at exceedance probability  $\alpha$  both have a total exceedance probability of  $\alpha$ . Therefore, if the hypothetical, fully optimized structure is designed using directional criteria derived from ISORM or HD contours then the failure probability will be equal to the contour exceedance probability (under the assumption of a deterministic response dependent on  $H_s$  and  $\Theta$  only). Feld *et al.* [42] note that there are infinitely many ways to define directional criteria which achieve the target reliability for the structure. The use of ISORM or HD contours represent two methods to achieve this. In particular, the ISORM contour corresponds to directional return values with equal return periods, advocated by Forristall [41], whereas the HD contour corresponds to the smallest possible region in the variable space to contain  $1 - \alpha$  probability.

In reality no structure will be fully optimized in each direction. Instead, there could be a single direction where exceeding the directional criteria leads to failure, but in other directions a non-zero margin exists until failure occurs. In such a case the probability of failure of a structure that is designed based on an HD and ISORM design conditions will be smaller than the target failure probability. Consider the simple example that the structure is designed to have a smaller response in the  $x'$ -direction than the  $y'$ -direction (where  $x'$  and  $y'$  represent a local coordinate system of the

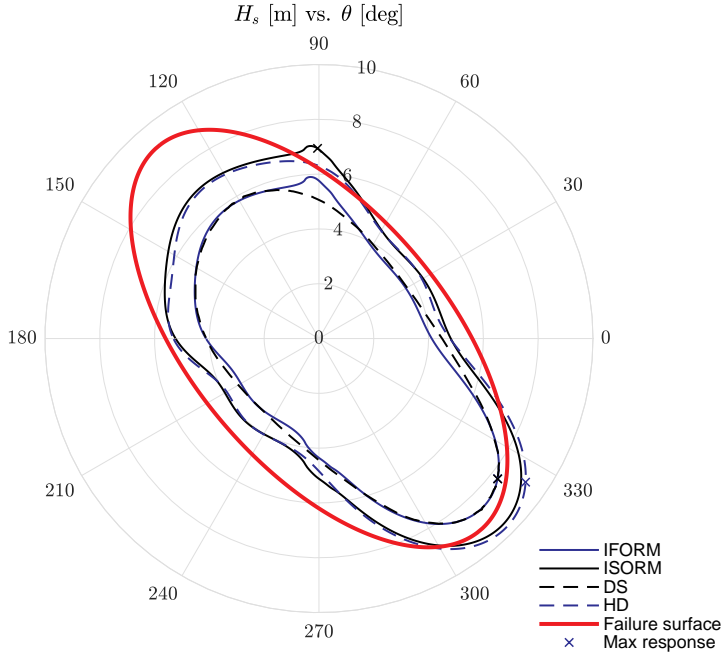


Figure 17: 1-year environmental contours for joint distribution of  $H_s$  and wave direction. The failure surface is defined by assuming that failure occurs when the response function (Equation 23) exceeds the true 1-year response such that the failure region contains a probability of exactly  $\alpha$ . Note that the IFORM and DS contours are fully contained within the survival region.

Method	1-year response	Sea state causing 1-year response ( $h_s, \theta$ )	$P_f$
IFORM contour	10.00	8.28 m, 322°	$2.11 \alpha$
DS contour	10.04	8.34 m, 322°	$1.98 \alpha$
ISORM contour	11.62	6.94 m, 90°	$0.11 \alpha$
HD contour	11.45	9.18 m, 325°	$0.15 \alpha$
All sea states approach	10.42	-	$\alpha$

Table 4: Structural responses from different contour methods for a system whose response depends on wave direction.  $P_f$  is the probability of failure of structure that is designed to have a capacity of the 1-year response.

structure). In this example we consider the following simple response function

$$r(h_{x'}, h_{y'}) = \sqrt{ah_{x'}^2 + bh_{y'}^2}, \quad (22)$$

where  $a = 1.3$  and  $b = 5$ . Or expressing this in the global coordinates,  $x, y$ , which are rotated by an angle  $\phi$  to the local coordinate system:

$$r(h_x, h_y) = \sqrt{a(h_x \cos \phi + h_y \sin \phi)^2 + b(-h_x \sin \phi + h_y \cos \phi)^2}. \quad (23)$$

Based on the distribution of  $H_s$  and  $\Theta$  we are considering here, suppose that the structure is designed such that its response is weakest in the direction where the highest waves occur such that  $\phi = 310^\circ$ . The 1-year response of this structure was calculated using the all sea state approach and using the four environmental contour methods. As expected, the IFORM and DS contours underestimate the 1-year response while the ISORM and HD contours overestimate it (see Table 4). The underestimation is approximately 4% for the IFORM and DS contours and the overestimation is approximately 10% for the ISORM and HD contours.

Suppose that the structure is designed such that its capacity is exactly the 1-year response estimated by a particular contour method such that, for example, in the case that an IFORM contour is used the capacity is 10.00, but if an ISORM contour is used the capacity is 11.62. In this case the probability of failure for IFORM and DS contours are roughly double the target probability of failure and the probability of failure for ISORM and HD contours are lower than the target probability of failure (roughly 7 and 9 times lower, respectively). So in this example, the use of IFORM or DS contours would be non-conservative, whilst using ISORM or HD contours would achieve the target reliability.

## 8. Conclusions

The differences between environmental contours defined in terms of marginal and total exceedance probabilities have been explored. For IFORM and ISORM contours the ratio between the marginal exceedance probability of the highest point along the contour and the total exceedance probability of the contour depends on the contour exceedance

probability and number of variables, but is independent of the joint distribution of variables. The marginal return period of the highest point along an ISORM contour in 2D, is approximately 10 times higher than the contour return period, whereas in 4D the marginal return period of the highest point along an ISORM contour is more than 200 times higher. The influence this has on the difference between the marginal return value at a given exceedance probability and the value of the highest point along an ISORM contour is dependent on the shape of the joint distribution, with longer-tailed distributions giving a larger change in the return value for a given change in the return period.

The relationship between marginal and total exceedance probabilities for direct sampling contours is dependent on the shape of the joint distribution of variables. However, in the case that the joint distribution has convex isodensity contours, the relationship between marginal and total exceedance probabilities is approximately equal to that for IFORM contours.

For highest density contours, the marginal exceedance probability of the highest point along the contour is not in fixed relationship with the total exceedance probability, but depends on the shape of the joint distribution of variables. In general we have  $c_\alpha > x_\alpha$  for HD contours in two or more dimensions.

The effect this has on structural reliability calculations is problem specific, with the impact depending on both the joint distribution of variables and the response function. In particular, the appropriate choice of contour is dependent on the shape of the failure surface. In the simple one-degree-of-freedom example presented in this paper, the failure surface was convex and the use of DS or IFORM contours was appropriate. In this case, the 50-year IFORM and DS contours gave an estimate of the 50-year response within 2% of the true 50-year response, whereas the HD and ISORM contours gave estimates that were 18% and 26% higher respectively. Clearly, this can have a significant implications for the design of a structure. In the second example, where directional design conditions are specified, the failure surface is concave in polar coordinates. In this case, the use of DS or IFORM contours resulted in non-conservative design conditions, whereas HD or ISORM contours preserved the intended reliability.

The results presented in this work emphasise the importance of having some understanding of the shape of the failure surface of a structure, so that the appropriate choice of environmental contour can be made.

## Data availability

The analysis of Example 1 and Example 2 can be reproduced by running the Matlab files `Example1.m` and `Example2.m` that are available at the GitHub repository <https://github.com/ahaselsteiner/2020-note-on-contours>. Matlab implementations of the IFORM, ISORM, DS and HD methods are available in the software package `compute-hdc` that is available at <https://github.com/ahaselsteiner/compute-hdc>.

## Acknowledgements

EM was funded under EPSRC grant EP/R007519/1.

## References

- [1] S. Haver, S. Winterstein, Environmental contour lines: A method for estimating long term extremes by a short term analysis, *Transactions - Society of Naval Architects and Marine Engineers* 116 (2009) 116–127.
- [2] E. Ross, O. C. Astrup, E. Bitner-Gregersen, N. Bunn, G. Feld, B. Gouldby, A. Huseby, Y. Liu, D. Randell, E. Vanem, P. Jonathan, On environmental contours for marine and coastal design, *Ocean Engineering* [doi:10.1016/j.oceaneng.2019.106194](https://doi.org/10.1016/j.oceaneng.2019.106194).
- [3] A. Naeff, T. Moan, *Stochastic Dynamics of Marine Structures*, Cambridge University Press, 2013.
- [4] J. H. J. Einmahl, L. D. Haan, A. Krajina, Estimating extreme bivariate quantile regions, *Extremes* 16 (2013) 121–145. [doi:10.1007/s10687-012-0156-z](https://doi.org/10.1007/s10687-012-0156-z).
- [5] F. Serinaldi, Dismissing return periods!, *Stochastic Environmental Research and Risk Assessment* 29 (4) (2015) 1179–1189. [doi:10.1007/s00477-014-0916-1](https://doi.org/10.1007/s00477-014-0916-1).
- [6] S. R. Winterstein, T. C. Ude, C. A. Cornell, P. Bjerager, S. Haver, Environmental parameters for extreme response: Inverse FORM with omission factors, in: Proc. 6th International Conference on Structural Safety and Reliability (ICOSSAR 93), Innsbruck, Austria, 1993.
- [7] A. B. Huseby, E. Vanem, B. Natvig, A new approach to environmental contours for ocean engineering applications based on direct Monte Carlo simulations., *Ocean Engineering* 60 (2013) 125–135.
- [8] W. Chai, B. J. Leira, Environmental contours based on inverse SORM, *Marine Structures* 60 (2018) 34–51.
- [9] A. F. Haselsteiner, J.-H. Ohlendorf, W. Wosniok, K.-D. Thoben, Deriving environmental contours from highest density regions, *Coastal Engineering* 123 (2017) 42–51.
- [10] E. Vanem, E. M. Bitner-Gregersen, Alternative environmental contours for marine structural design - a comparison study, in: 33rd International Conference on Ocean, Offshore and Arctic Engineering, 2014, pp. OMAE2014-23252. [doi:10.1115/OMAE2014-23252](https://doi.org/10.1115/OMAE2014-23252).
- [11] E. Vanem, A comparison study on the estimation of extreme structural response from different environmental contour methods, *Marine Structures* 56 (2017) 137–162.
- [12] E. Vanem, B. Guo, E. Ross, P. Jonathan, Comparing different contour methods with response-based methods for extreme ship response analysis, *Marine Structures* 69. [doi:10.1016/j.marstruc.2019.102680](https://doi.org/10.1016/j.marstruc.2019.102680).
- [13] S. Haver, Wave climate off northern Norway, *Applied Ocean Research* 7 (2) (1985) 85–92. [doi:10.1016/0141-1187\(85\)90038-0](https://doi.org/10.1016/0141-1187(85)90038-0).
- [14] J. Mathisen, E. Bitner-Gregersen, Joint distributions for significant wave height and wave zero-up-crossing period, *Applied Ocean Research* 12 (1990) 93–103.
- [15] L. Li, Z. Gao, T. Moan, Joint environmental data at five European offshore sites for design of combined wind and wave energy devices, in: 32nd International Conference on Ocean, Offshore and Arctic Engineering, 2013, pp. OMAE2013-10156. [doi:10.1115/OMAE2013-10156](https://doi.org/10.1115/OMAE2013-10156).

[16] A. F. Haselsteiner, A. Sander, J.-H. Ohlendorf, K.-D. Thoben, Global hierarchical models for wind and wave contours: Physical interpretations of the dependence functions, in: 39th International Conference on Ocean, Offshore and Arctic Engineering, American Society of Mechanical Engineers (ASME), 2020.

[17] R. Montes-Iturriaga, E. Heredia-Zavoni, Environmental contours using copulas, *Applied Ocean Research* 52 (2015) 125–139.

[18] R. Montes-Iturriaga, E. Heredia-Zavoni, Multivariate environmental contours using C-vine copulas, *Ocean Engineering* 118 (2016) 68–82.

[19] L. Manuel, P. T. Nguyen, J. Canning, R. G. Coe, A. C. Eckert-Gallup, N. Martin, Alternative approaches to develop environmental contours from metocean data, *Journal of Ocean Engineering and Marine Energy* 4 (2018) 293–310.

[20] T. Fazeres-Ferradosa, F. Taveira-Pinto, E. Vanem, M. T. Reis, L. das Neves, Asymmetric copula-based distribution models for met-ocean data in offshore wind engineering applications, *Wind Engineering* 42 (2018) 304–334.

[21] A. Eckert-Gallup, N. Martin, Kernel density estimation (KDE) with adaptive bandwidth selection for environmental contours of extreme sea states, in: OCEANS 2016 MTS/IEEE, 2016, pp. 1–5.

[22] A. Haselsteiner, J.-H. Ohlendorf, K.-D. Thoben, Environmental contours based on kernel density estimation, in: 13th GermanWind Energy Conference DEWEK, 2017.

[23] P. Jonathan, J. Flynn, K. C. Ewans, Joint modelling of wave spectral parameters for extreme sea states, *Ocean Engineering* 37 (2010) 1070–1080.

[24] P. Jonathan, K. Ewans, J. Flynn, On the estimation of ocean engineering design contours, *Journal of Offshore Mechanics and Arctic Engineering* 136. doi:10.1115/1.4027645.

[25] H. F. Hansen, D. Randell, A. R. Zeeberg, P. Jonathan, Directional seasonal extreme value analysis of North Sea storm conditions, *Ocean Engineering* 195 (2020) 106665. doi:10.1016/j.oceaneng.2019.106665. URL <https://doi.org/10.1016/j.oceaneng.2019.106665>

[26] E. B. L. Mackay, P. Jonathan, Estimation of environmental contours using a block resampling method, in: 39th International Conference on Ocean, Offshore and Arctic Engineering, 2020, pp. OMAE2020–18308.

[27] S. Haver, On the joint distribution of heights and periods of sea waves, *Ocean Engineering* 14 (5) (1987) 359–376. doi:10.1016/0029-8018(87)90050-3.

[28] NORSO, Standard N-003: Actions and action effects, Tech. rep. (2007).

[29] DNVGL, Recommended practice DNVGL-RP-C205: Environmental conditions and environmental loads, Tech. rep. (2019).

[30] Q. Derbanne, G. de Hauteclercque, A new approach for environmental contour and multivariate de-clustering, in: 38th International Conference on Ocean, Offshore and Arctic Engineering, Glasgow, 2019, p. OMAE2019/95993. doi:10.1115/OMAE2019-95993.

[31] H. O. Madsen, S. Krenk, N. C. Lind, Methods of structural safety, Dover Publications, Mineola, New York, USA, 2006.

[32] M. Rosenblatt, Remarks on a multivariate transformation, *Ann. Math. Statistics* 23 (1952) 470–472.

[33] R. J. Hyndman, Computing and graphing highest density regions, *The American Statistician* 50 (2) (1996) 120–126.

[34] E. Vanem, E. M. Bitner-Gregersen, Stochastic modelling of long-term trends in the wave climate and its potential impact on ship structural loads, *Applied Ocean Research* 37 (2012) 235–248. doi:10.1016/j.apor.2012.05.006.

[35] C. Armstrong, A. Waterhouse, C. Chin, Y. Drobyshevski, Investigation into application of environmental contours for analysis of floating systems, in: Proc. 13th Pacific-Asia Offshore Mechanics Symposium, International Society of Offshore and Polar Engineers (ISOPPE), Jeju, Korea, 2018, pp. 470–477.

[36] O. Faltinsen, *Sea Loads on Ships and Offshore Structures*, Cambridge University Press, 1990.

[37] D. Randell, G. Feld, K. Ewans, P. Jonathan, Distributions of return values for ocean wave characteristics in the South China Sea using directional-seasonal extreme value analysis, *Environmetrics* 26 (6) (2015) 442–450. doi:10.1002/env.2350.

[38] M. Jones, D. Randell, K. Ewans, P. Jonathan, Statistics of extreme ocean environments: Non-stationary inference for directionality and other covariate effects, *Ocean Engineering* 119 (2016) 30–46. doi:10.1016/j.oceaneng.2016.04.010.

[39] Z. S. Haghayeghi, M. J. Ketabdar, Development of environmental contours for circular and linear metocean variables, *International Journal of Renewable Energy Research* 7 (2) (2017) 682–693.

[40] E. Vanem, A. Hafver, G. Nalvar, Environmental contours for circular-linear variables based on the direct sampling method, *Wind Energy* (October) (2019) 1–12. doi:10.1002/we.2442.

[41] G. Z. Forristall, On the Use of Directional Wave Criteria, *Journal of Waterway, Port, Coastal, and Ocean Engineering* 130 (5) (2004) 272–275.

[42] G. Feld, P. Jonathan, D. Randell, On the estimation and application of directional design criteria, in: 38th International Conference on Offshore Mechanics and Arctic Engineering, 2019. doi:10.1115/OMAE2019-96586.